Chapter 3

Transmission Line Model of a Dual-band Metamaterial Absorber

3.1 Introduction

Metamaterial absorber structures are usually designed and analyzed using various numerical techniques (like MoM, FDTD, FEM, etc.) based commercial electromagnetic solvers utilizing periodic boundary conditions which incorporates the coupling effects of nearby placed unit cells into the calculation. These calculations are fast, robust, and accurate based on the proper meshing criteria. However, to get the good physical insight of the resonance behavior of such structures, equivalent circuit modeling is often desired.

Equivalent circuit model of the basic frequency selective surfaces (FSS) forming the absorber top layer like loop [Langley and Parker (1982)], patch [Pang *et al.* (2011)], Jerusalem cross [Costa *et al.* (2014)] was studied in the literature. These basic geometries support single band absorption behavior. Nested square loop and nested circular loop providing multiband absorption behavior were also modeled effectively [Shang *et al.* (2013), Langley and Parker (1983), Bhattacharyya *et al.* (2014)]. However, difficulty arises in modeling the complex geometries. The circuit model of the resonator without incorporating the coupling effects of the periodic structure was presented in [Pang *et al.* (2013)]. In [Zhong *et al.* (2012), Mao *et al.* (2014), Ghosh *et al.* (2014)], the equivalent circuit model was presented for typical resonators without quantitatively analyzing the various equivalent circuit components of the unit cells.

In this chapter, the equivalent circuit is proposed using transmission line model for the dual-band metamaterial absorber presented in chapter 2 considering the normal

incidence of the wave. Peak absorptivity of 95.02% and 99.84% are obtained at 4.215 GHz and 10.95 GHz, respectively. All the coupling capacitances of the periodic structure are included in the proposed equivalent circuit model. The metamaterial absorber utilizes frequency selective surface (FSS) printed on a grounded dielectric material. The presented absorber structure consists of square patch inside a closed ring resonator as FSS, and the two geometries are connected to each other at the corners. The proposed circuit model is based on the surface current distribution obtained through simulation. The simulated reflection response of the proposed structure was already verified by the experimental response in the previous chapter (chapter 2). Therefore, the simulated response is taken as a reference to obtain the values of the lumped elements present in the analytical model.

The FSS of the presented structure is first decomposed in two simpler FSS and the two absorber structures are formed utilizing these FSSs. The circuit model for these individual absorber structures is proposed and verified through simulation. Now, the proposed circuit models of the two individual structures are combined to obtain the equivalent circuit model of the proposed absorber structure by taking all the coupling capacitances into consideration. A good agreement is observed between the analytical and simulated results. The general transmission line model of the metamaterial absorber structure is presented in section 3.2. Section 3.3 illustrates the proposed equivalent circuit model of the proposed absorber structure. The values of involved lumped parameters are also calculated in this section. The conclusion of the chapter is provided in section 3.4.

3.2 General Transmission Line Model of the Metamaterial Absorber

The side view of the three-layered structure of the metamaterial absorber is shown in Figure 3.1 along with its transmission line model. The dielectric substrate is represented

by the transmission line of length '*t*'. One end of the transmission line is connected to the FSS impedance, Z_{FSS}, while another end is shorted representing the presence of the complete metallic backplane as ground. The input impedance of shorted transmission line Z_d is given by Equation 3.1 and appears in parallel to the Z_{FSS}.

$$Z_d = j\frac{Z_0}{\sqrt{\varepsilon_r}} tan(k_0\sqrt{\varepsilon_r}t) \tag{3.1}$$

where ε_r is the permittivity of the dielectric substrate and is given as $\varepsilon_r = \varepsilon_r' - j\varepsilon_r''$. Z_0 and k_0 are the free space impedance and free space propagation constant, respectively.

For minimum reflections from the metamaterial absorber, the total impedance Z_T (Equation 3.2) must be matched to the free space impedance Z_0. The reflection coefficient (S_{11}) of the structure is obtained from Equation 3.3.

$$Z_T = Z_{FSS} \text{ P} Z_d = \frac{Z_{FSS}Z_d}{Z_{FSS} + Z_d} \tag{3.2}$$

$$S_{11} = \frac{Z_T - Z_0}{Z_T + Z_0} \tag{3.3}$$

For perfect absorption, the reflection coefficient of the structure should be zero, and hence the $Re(Z_T)$ should be equal to Z_0 and $Im(Z_T)$ should have smoothed transition from zero at the frequency of absorption. The method of obtaining the Z_{FSS} for the proposed absorber structure is discussed in the next section.

3.3 Equivalent Circuit Model of the Proposed Absorber

The FSS of the proposed absorber is considered as being constructed of the combination of two simpler structures as shown in Figure 3.2 for the ease of the analysis. The first FSS consists of a square-shaped closed ring resonator (CRR) and the second FSS is made up of square patch along with the diagonal arms. The two FSSs are termed as

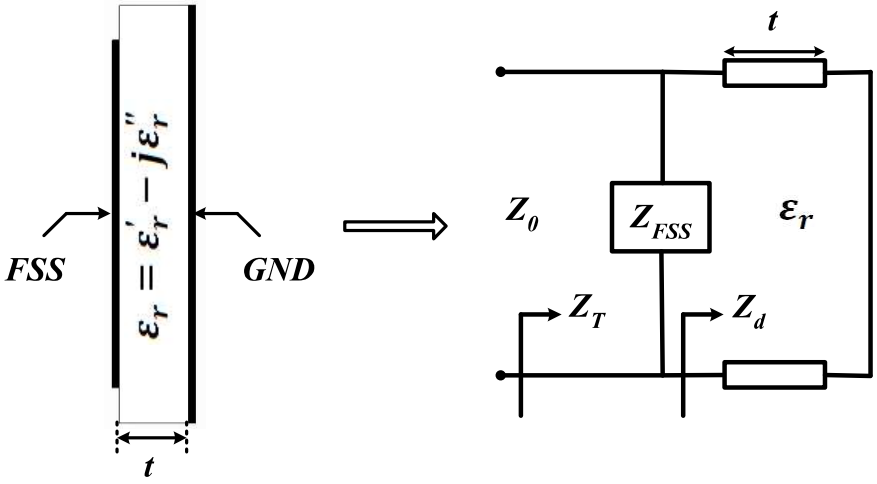

Figure 3.1: Side view of the MTM absorber and its transmission line equivalent model.

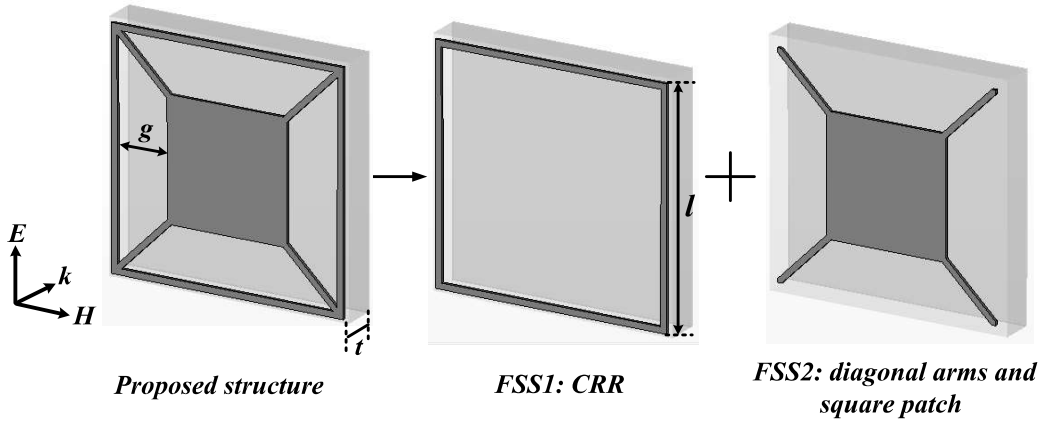

Figure 3.2: Decomposition of the proposed FSS into simpler structures (t = 0.8 mm and l = 11.6 mm).

FSS1 and FSS2 and the corresponding absorber structures utilizing these FSSs as resonator are termed as absorber1 and absorber2, respectively in the rest of the chapter.

The equivalent circuits of absorber1 and absorber2 are presented separately, and corresponding reflection coefficients are calculated using Equations 3.1–3.3. The calculated reflection response is compared with the simulated reflection response to validate the conceived equivalent circuit models. Now, the impedance of the FSS1 (Z_{FSS1}) and FSS2 (Z_{FSS2}) are combined in a suitable manner to get the impedance of the

proposed FSS (Z_{FSS}) which in turn provides the reflection response of the proposed absorber structure.

3.3.1 Modeling of the Absorber1:

The surface current direction along FSS1 and its neighboring unit cells is presented in Figure 3.3 for the normally incident plane wave. It is observed that the CRR edge 1 and 3 are coupled to the edges of the neighboring CRR by even mode coupling as the direction of current is same, while CRR edges 2 and 4 are having odd mode coupling to its neighboring CRR edges as the flow of current is in the opposite direction. The even and odd mode coupling introduces two coupling capacitances C_e and C_o, which consists of the parallel plate (C_p) and fringing capacitances (C_f, C_{f1}, C_{ga}, and C_{gd}) of the coupled microstrip lines. The C_e and C_o can be represented as shown in Figs. 3.4(a) and (b), respectively, and are defined per unit length of the microstrip line. The values of the C_e and C_o for a microstrip line of width W, height t, impedance Z_0, and effective dielectric constant ε_{re} are evaluated using Eqs. 3.4 and 3.5, respectively [Garg and Bahl (1979)].

$$C_e = C_p + C_f + C_{f1} \tag{3.4}$$

$$C_o = C_p + C_f + C_{ga} + C_{gd} \tag{3.5}$$

where parallel plate capacitance C_p is given by Equation 3.6.

$$C_p = \frac{\varepsilon_0 \varepsilon_r W}{t} \tag{3.6}$$

The fringing capacitance of the microstrip line, C_f is given by Equation 3.7.

$$2C_f = \frac{\sqrt{\varepsilon_{re}}}{cZ_0} - C_p \tag{3.7}$$

where c is the velocity of light in free space.

The term C_{f1} represent the modification in fringing capacitance of a microstrip line in the presence of another line and is evaluated by the empirical expression given by Equation 3.8 [Garg and Bahl (1979)].

$$C_{f1} = \frac{C_f}{1 + A(t/S)\tanh(8S/t)} \tag{3.8}$$

where S is the gap in between the two coupled microstrip line and,

$$A = exp[-0.1exp(2.33 - 2.53W/t)] \tag{3.9}$$

C_{ga} and C_{gd} are the fringing capacitances across the gap S, in the air and dielectric region, respectively. C_{ga} and C_{gd} are evaluated using Equations 3.10–3.12.

$$C_{ga} = \varepsilon_0 \frac{K(k')}{K(k)}, k = \frac{S/t}{S/t + 2W/t}, \; k' = \sqrt{1-k^2} \tag{3.10}$$

where $K(k)$ is the complete elliptic function and $K(k')$ is its complement and their ratio is given as [Garg and Bahl (1979)],

$$\frac{K(k')}{K(k)} = \begin{cases} \frac{1}{\pi} ln\left[2\frac{1+\sqrt{k'}}{1-\sqrt{k'}}\right], & 0 \le k^2 \le 0.5 \\ \frac{\pi}{ln\left[2\frac{1+\sqrt{k}}{1-\sqrt{k}}\right]}, & 0.5 \le k^2 \le 1 \end{cases} \tag{3.11}$$

and,

$$C_{gd} = \frac{\varepsilon_0 \varepsilon_r}{\pi} ln\left\{coth\left(\frac{\pi}{4}\frac{S}{t}\right)\right\} + 0.65C_f\left[\frac{0.02}{S/t}\sqrt{\varepsilon_r} + 1 - \frac{1}{\varepsilon_r^2}\right] \tag{3.12}$$

Based on the surface current, the equivalent circuit of the FSS1 is shown in Figure 3.4(c). C_{el} and C_{ol} are the even and odd mode coupling capacitance corresponding to the length l of the CRR. The inductance per unit length (L) is obtained from the quasi-static analysis of the microstrip line as given in Equation 3.13 [Gupta *et al.* (1996)], and corresponding FSS inductance for length l of the CRR is calculated (L_l).

$$L = \frac{Z_0\sqrt{\varepsilon_{re}}}{c} \tag{3.13}$$

The calculated values of the lumped elements are as: L_l = 7.11 nH, C_{el} = 0.51 pF, C_{ol} = 1.01 pF. Additional inductance and capacitance correspond to the right angle bending of the microstrip line are included in the analysis. The right angle bend is expressed as equivalent T-network as shown in Figure 3.5 and the closed-form expressions for the corresponding capacitance and inductance are as given in Equation 3.14 and 3.15[Gupta *et al.* (1996)].

$$\frac{C_b}{W}(pF/m) = \begin{cases} \dfrac{(14\varepsilon_r + 12.5)W/t - (1.83\varepsilon_r - 2.25)}{\sqrt{W/t}} + \dfrac{0.02\varepsilon_r}{W/t} & for\ W/t < 1 \\ (9.5\varepsilon_r + 1.25)W/t + 5.2\varepsilon_r + 7 & for\ W/t \geq 1 \end{cases} \tag{3.14}$$

$$\frac{L_b}{t}(nH/m) = 100\left\{4\sqrt{\frac{W}{t}} - 4.21\right\} \tag{3.15}$$

The effect of the finite thickness of the metallization t_m (= 35 μm) in the structure is also taken into calculations using the concept of the effective width of the microstrip line, W_t. The effective width is calculated for even and odd mode coupling using Equation 3.16-3.18 [Jansen (1978)]. These expressions are valid for $S \geq 2t_m$.

$$\frac{W_t^e}{t} = \frac{W}{t} + \frac{\Delta W}{t}\left[1 - 0.5\,exp\left(-0.69\,\Delta W/\Delta t\right)\right] \tag{3.16}$$

$$\frac{W_t^o}{t} = \frac{W_t^e}{t} + \frac{\Delta t}{t} \tag{3.17}$$

where,

$$\frac{\Delta t}{t} = \frac{1}{\varepsilon_r}\frac{t_m/t}{S/t} \tag{3.18}$$

and ΔW is the increase in width of the single microstrip line due to finite thickness of the metallization, t_m, and is given as in Equation 3.19 [Hammerstad and Bekkadal (1975)].

$$\Delta W = \begin{cases} \dfrac{t_m\left(1+ln\left(\dfrac{2t}{t_m}\right)\right)}{\pi}, & W > \dfrac{t}{2\pi} > 2t_m \\ \dfrac{t_m\left(1+ln\left(\dfrac{4\pi W}{t_m}\right)\right)}{\pi}, & \dfrac{t}{2\pi} > W > 2t_m \end{cases} \tag{3.19}$$

The losses in the structure are included in the equivalent circuit model as resistance R_{l1}. R_{l1} is a series combination of resistors R_o and R_d that corresponds to the ohmic and dielectric losses, respectively. Resistance R_o is given by Equation 3.20 [Costa *et al.* (2013)].

$$\mathrm{R_o} = \frac{\text{cell area}}{\text{metallized area of FSS}}\left(\frac{1}{\delta\sigma}\right) \tag{3.20}$$

where, δ and σ are the skin depth and conductivity of the metal, and the quantity present in the bracket is the surface resistance of the metal. The calculation of R_d involves the unloaded capacitance of the FSS which could be obtained either from the simulated data itself or from the closed-form expressions of the FSS, if available [Costa *et al.* (2013)]. To avoid the cumbersome calculation of R_d, it is taken as a variable resistor which can be tuned to get the absorption level and bandwidth.

The impedance (Z_{FSS1}) is calculated across the terminal 1-2 of the equivalent circuit presented in Figure 3.4(c) and then the reflection coefficient of the absorber1 is calculated using Equations 3.1–3.3. The calculated and simulated reflection response is compared in Figure 3.6. The calculated and simulated peak absorption frequencies are observed at 3.08 GHz and 3.135 GHz, respectively. A close agreement is observed in

the peak absorption frequencies with a slight deviation of 1.75%. The deviation is due to the inherent error involved in the empirical formulae used for the analysis.

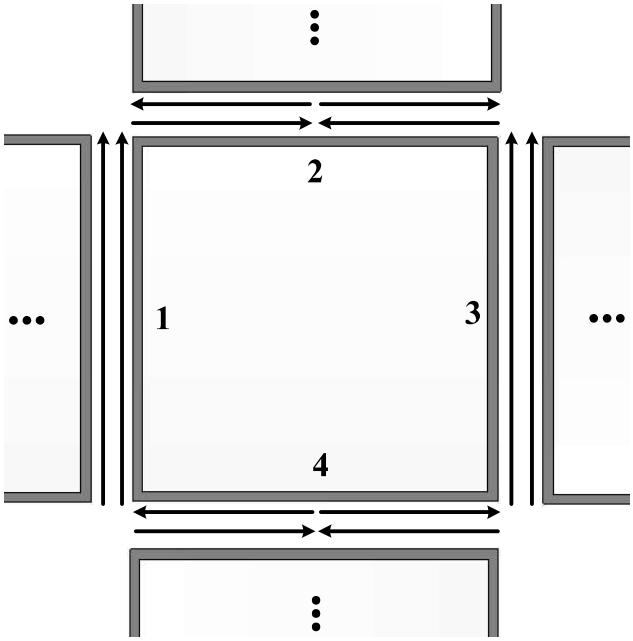

Figure 3.3: Surface current directions in the periodic square-shaped CRR structure.

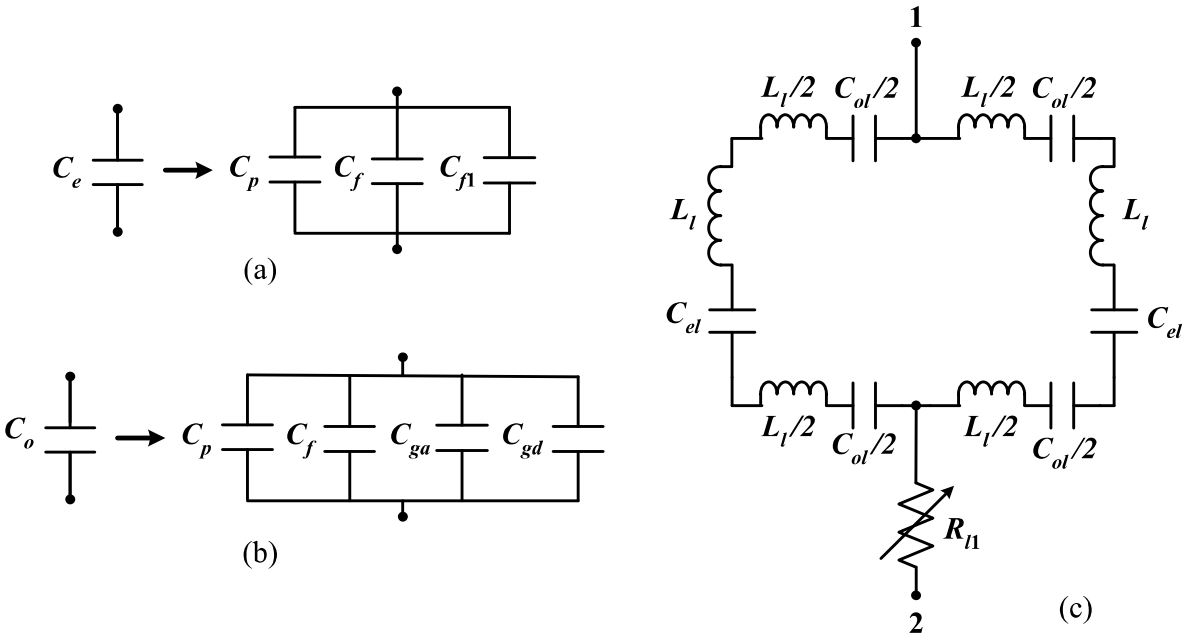

Figure 3.4: (a) Even and (b) odd mode coupling capacitance, (c) equivalent circuit of the FSS1.

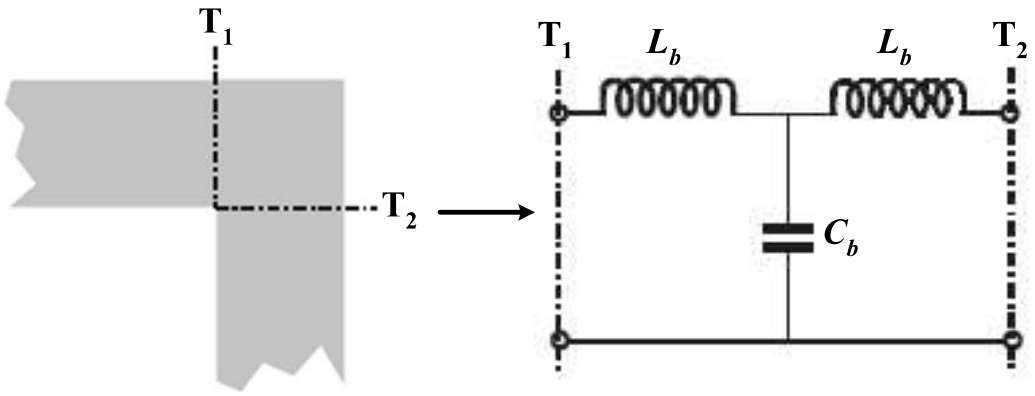

Figure 3.5: Microstrip bend and its equivalent T-network.

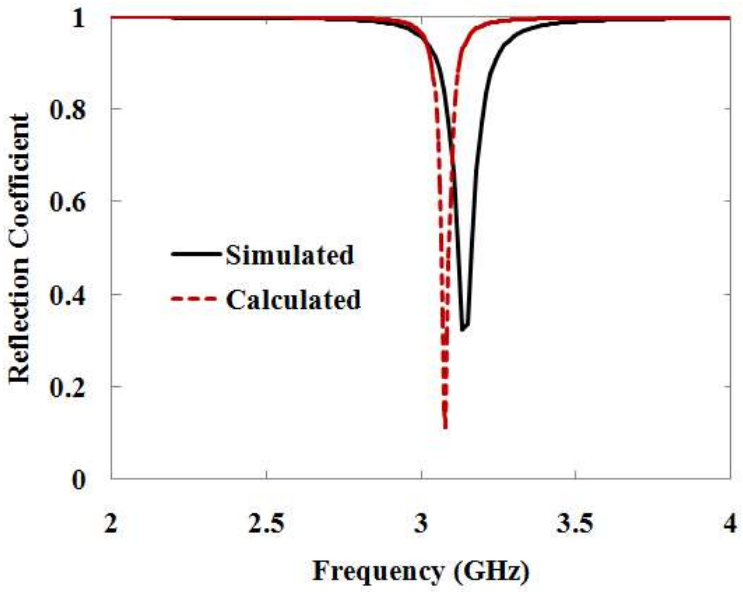

Figure 3.6: Reflection response of the absorber1.

3.3.2 Modeling of the Absorber2:

Absorber2 is designed using FSS2 as the top layer keeping all other parameters constant. The proposed equivalent circuit of the FSS2 is shown in Figure 3.7. L_d and C_d are the lumped inductance and capacitance of the diagonal arm. L_{sp} and C_{sp} are the lumped inductance and capacitance of the square patch. The values of lumped inductance (L) and capacitance (C) per unit length of the microstrip line are calculated

using quasi-static analysis of the microstrip line [Gupta *et al.* (1996)] using Equation 3.13 and 3.21, respectively.

$$C = \frac{\sqrt{\varepsilon_{re}}}{cZ_0} \tag{3.21}$$

The corresponding values of the various lumped parameters are as follows: L_d = 2.019 nH, C_d = 0.204 pF, L_{sp} = 0.721 nH, C_{sp} = 2.077 pF. Since quasi-static analysis utilizes the concept of effective dielectric constant and hence, the effect of fringing has already been taken into account. R_{l2} represents the losses in the structure and is a combination of resistors representing ohmic and dielectric losses as discussed before. Since metamaterial absorbers are the periodic structures, therefore, effective coupling capacitance C_c appears in the equivalent circuit model because of the close proximity of a unit cell with its neighboring unit cells. The value of the C_c is calculated using the resonance condition of the metamaterial absorber. At resonance $X = -B$, where X and B are the imaginary parts of the two complex impedances Z_{FSS2} (calculated at node 3-4 of Figure 3.7) and Z_d (impedance of grounded dielectric substrate), respectively, as given in Equation 3.22 and 3.23 [Costa *et al.* (2013)].

$$Z_{FSS2} = R_{l2} + jX \tag{3.22}$$

$$Z_d = A + jB \tag{3.23}$$

The calculated value of C_c is 0.403 pF. Based on the extracted lumped element values, the reflection coefficient of the absorber2 is calculated and compared with the simulated reflection response in Figure 3.8. A close match justifies the reliability of the extracted values. The bandwidth and the absorption level could be adjusted by tuning the resistance R_{l2}.

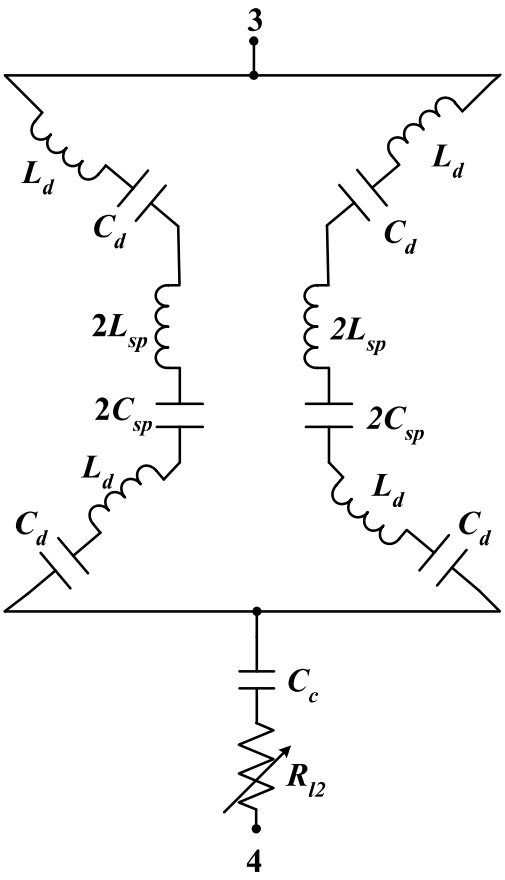

Figure 3.7: Equivalent circuit of the FSS2.

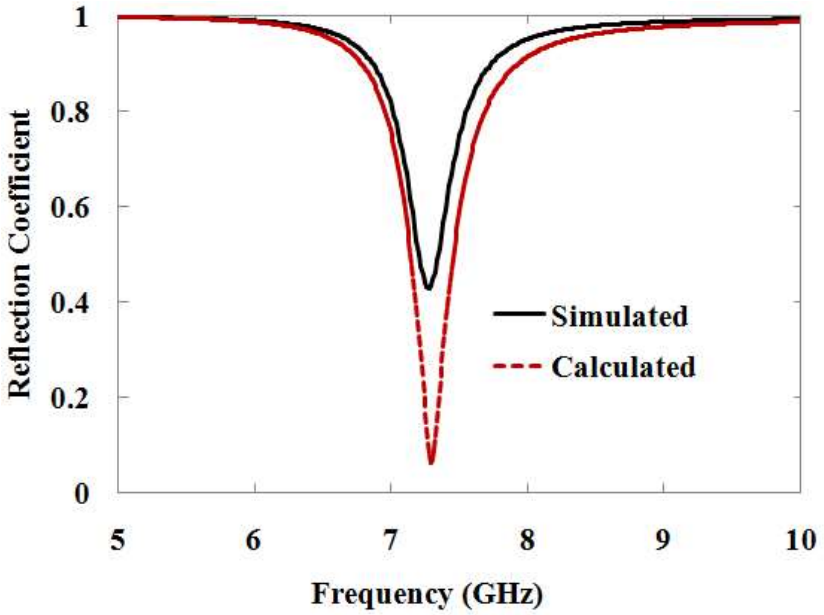

Figure 3.8: Reflection response of the absorber2.

3.3.3 Modeling of the Proposed Absorber

The two individual FSS (FSS1 and FSS2) are combined together to form the FSS of the proposed absorber structure. It is observed from Figure 3.6 and Figure 3.8 that the absorber1 and absorber2 resonates at 3.135 GHz and 7.275 GHz, while, resonance frequencies are shifted to 4.215 GHz and 10.95 GHz, respectively on combining the FSS1 and FSS2 together in the proposed absorber. Therefore, the equivalent circuit model of the individual absorber structures employing FSS1 and FSS2 as top layer perturbed together when connected to form a single unit cell. The fringing fields of the FSS1 and FSS2 affect each other due to the finite gap '*g*' between them (see Figure 3.2). For its better understanding, the direction of the surface current induced on the absorber top layer for the normally incident wave is observed and presented in Figure 3.9. The surface current is plotted at the frequency (7 GHz) away from the frequency of absorption so that sufficient surface current gets induced at both the resonators (FSS1 and FSS2) simultaneously in a manner similar to that presented in [Bhattacharyya *et al.* (2014)]. The resonator arms with surface current in the opposite direction are having positive mutual coupling while the resonator arms with surface current in the same direction are having negative mutual coupling. An equivalent circuit model of the absorber structure is proposed in Figure 3.10 taking these mutual coupling into account. Effective coupling capacitances C_{c1} and C_{c2} are introduced in the proposed equivalent circuit model to account for the effect of coupling of FSS2 on FSS1 and FSS1 on FSS2, respectively. The FSS impedance (Z_{FSS}) is calculated at node 5-6, and corresponding reflection response is obtained and presented in Figure 3.11. The coupling capacitances C_{c1} and C_{c2} are tuned in such a way that to get a match between the simulated and calculated reflection response. The optimized values of C_{c1} and C_{c2} are 0.385 pF and 0.106 pF, respectively.

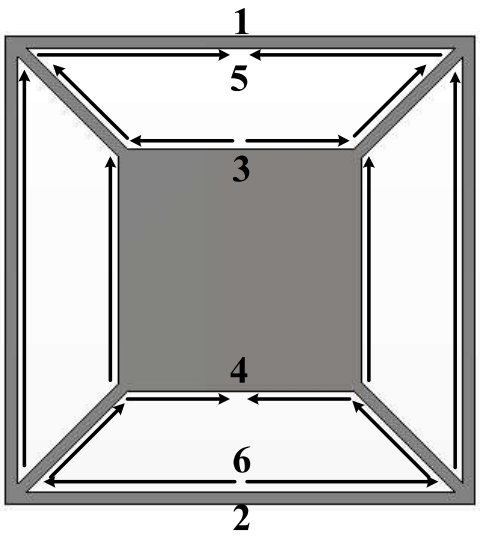

Figure 3.9: Surface current direction on the absorber top layer at 7 GHz (nodes 1-2: for FSS1, nodes 3-4: for FSS2, nodes 5-6: for proposed FSS).

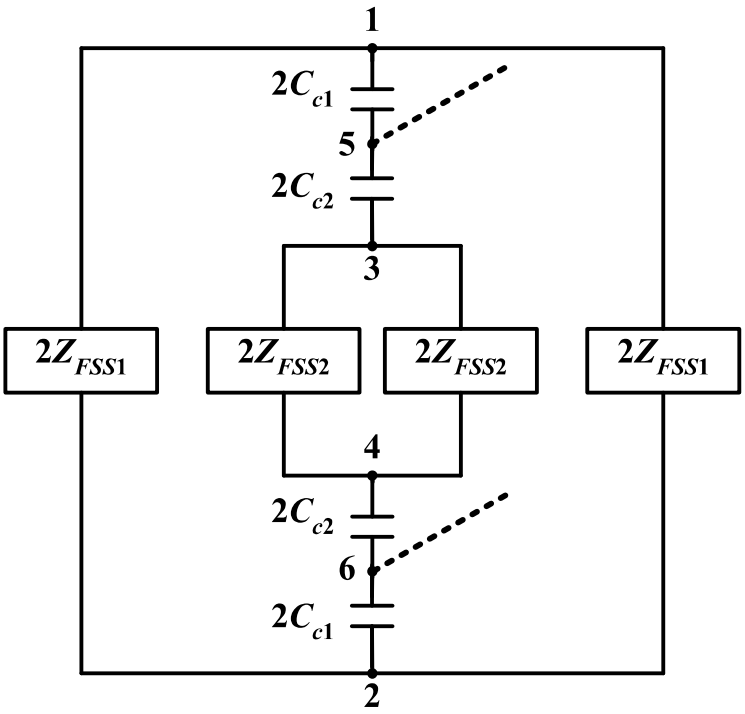

Figure 3.10: Proposed equivalent circuit model of the FSS used in dual-band absorber structure.

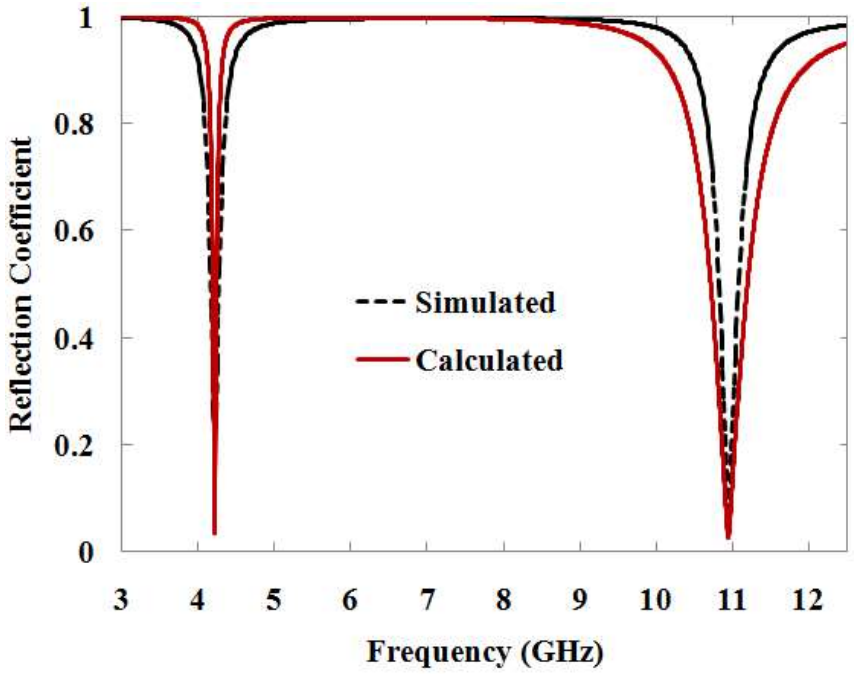

Figure 3.11: Simulated and calculated reflection response of the proposed absorber structure.

3.4 Conclusion

A transmission line model of the polarization-insensitive dual-band metamaterial absorber has been presented. Simulated reflection response was taken as a reference to compare the analytical results. The RLC model of the proposed FSS was developed by combining the RLC model of the two simpler FSS in which the proposed FSS was decomposed. Involved coupling capacitances have been calculated to get a correct match in the analytical and simulated results. The presented equivalent circuit model would pave the way in getting the good physical insight of the resonance phenomenon of the presented structure.

After numerically, analytically and experimentally investigating the dual-band metamaterial absorber in the present and previous chapters, a variant of the proposed resonator is studied to design and develop quad-band metamaterial absorber in the next chapter.

Left Intentionally